Femtosecond laser nanoaxotomy properties and their effect on axonal recovery in *C. elegans*.

Frederic Bourgeois and Adela Ben-Yakar

Mechanical Engineering, University of Texas at Austin,
1 University Station C2200, Austin TX 78712
ben-yakar@mail.utexas.edu

http://www.me.utexas.edu/ben-yakar/

Abstract: We present a study characterizing the properties of femtosecond laser nanosurgery applied to individual axons in live *Caenorhabditis elegans* (*C. elegans*) using nano-Joule laser pulses at 1 kHz repetition rate. Emphasis is placed on the characterization of the damage threshold, the extent of damage, and the statistical rates of axonal recovery as a function of laser parameters. The ablation threshold decreases with increasing number of pulses applied during nanoaxotomy. This dependency suggests the existence of an incubation effect. In terms of extent of damage, the energy per pulse is found to be a more critical parameter than the number of pulses. Axonal recovery improves when surgery is performed using a large number of low energy pulses.

OCIS codes: (140.7090) Ultrafast lasers; (170.1020) Ablation of tissue; (190.4180) Multiphoton processes.

References and links

1. P.J. Horner and F.H. Gage, "Regenerating the damaged central nervous system," Nature **407**, 963-970 (2000).
2. M. Kerschensteiner, M.E. Schwab, J.W. Lichtman and T. Misgeld, "In vivo imaging of axonal degereneration and regeneration in the injured spinal cord," Nature Med. **11(5)**, 572-577 (2005).
3. D.H. Bhatt, S.J. Otto, B. Depoister and J.R. Fetcho, "Cyclic AMP-induced repair of zebrafish spinal circuits," Science **305**, 254-258 (2004).
4. W.B. Wood, S. Brenner, R.K. Herman, S.W. Emmons, J. White, J. Sulston, H.R. Horvitz, J. Kimble, S. Ward, J. Hodgkin, R.H. Waterston, M. Chalfie and D.L. Riddle, *The nematode Caenorhabditis elegans*, (Cold Spring Harbor, 1988).
5. M.F. Yanik, H. Cinar, H.N. Cinar, A.D. Chisholm, Y. Jin and A. Ben-Yakar, "Functional regeneration after laser axotomy," Nature **432**, 882 (2004).
6. M.D. Perry, D.C. Stuart, P.S. Banks, M.D. Feit, V. Yanovsky and A.M. Rubenchik, "Ultrashort-pulse laser machining of dielectric materials," J. Appl. Phys. **85**, 6803-6810 (1999).
7. V. Venugopalan, A. Guerra III, K. Hahen and A. Vogel, "Role of laser-induced plasma formation in pulse cellular microsurgery and micromanipulation," Phys. Rev. Lett. **88**, 078103 (2002).
8. A. Vogel, J. Noack, G. Hüttman and G. Paltauf, "Mechanisms of femtosecond laser nanosurgery of cells and tissues," App. Phys. B, 10.1007 (2005).
9. K. König, W. Riemann and W. Fritzsche, "Nanodissection of human chromosomes with near-infrared femtosecond laser pulses," Opt. Lett. **26**, 819-821 (2001).
10. U.K. Tirlapur and K. König, "Targeted transfection by femtosecond laser," Nature **418**, 290-291 (2002).
11. N. Shen, D. Datta, C.B. Schaffer, P. LeDuc, D.E. Ingber and E. Mazur, "Ablation of cytoskeletal filaments and mitochondria in cells using a femtosecond laser nanocissor," Mech. Chem. Biosyst. **2**, 17 (2005).
12. A. Heisterkamp, I. Zaharieva Maxwell, E. Mazur, J. M. Underwood, J. A. Nickerson, S. Kumar and D. E. Ingber, "Pulse energy dependence of subcellular dissection by femtosecond laser pulses," Opt. Express **13**, 3690-3696 (2005).
13. S.H. Chung, D.A. Clark, C.V. Gabel, E. Mazur and A.D.T. Samuel, "The role of the AFD neuron in *C. elegans* thermotaxis analyzed using femtosecond laser ablation," BMC Neuro. **7**:30 (2006).
14. W. Watanabe and N. Arakawa, "Femtosecond laser disruption of subcellular organelles in a living cell," Opt. Express 12 (18), 4203-4213 (2004).
15. S. Brenner, "The genetics of behaviour," Brit. Med. Bull. **29**, 269-271 (1973).
16. X. Huang, H.J. Cheng, M. Tessier-Lavigne, Y. Jin, "MAX-1, a novel PH/MyTH4/FERM domain cytoplasmic protein implicated in netrin-mediated axon repulsion" Neuron **34**, 563-576 (2002).

17. J.G. White, F. Southgate, J.N. Thomson and S. Brenner, "The structure of the nervous system of the nematode Caenorhabditis elegans." Phil. Trans. Royal Soc. London Series B. Bio. Scien. **314**, 1-340 (1986).
18. M. Chalfie, "The differentiation and function of the touch receptor neurons of Caenorhabditis elegans" Prog. Brain. Res. **105**, 179-82 (1995).
19. M. Driscoll and M. Chalfie, "The mec-4 gene is a member of a family of Caenorhabditis elegans genes that can mutate to induce neuronal degeneration." Nature **349**, 588-593 (1991).
20. H. Urey, "Spot size, depth of focus and diffraction ring intensity formulas for truncated Gaussian beams." App. Phys. 43 (3), 620-625 (2004).
21. J.B. Guild, C. Xu and W.W. Webb, "Measurement of group delay dispersion of high numerical aperture objective lenses using two-photon excited fluorescence" Appl. Opt. **36** (1), 397-401 (1997).
22. F. Yanik, H. Cinar, N. Cinar, A. Chisholm, Y. Jin and A. Ben-Yakar, "Nerve regeneration in *Caenorhabditis elegans* after femtosecond laser axotomy." IEEE J. of Sel. Top. in Quan. Elect., Vol.12 No.6 (2006).
23. A. Waller, "Experiments on the section of glossopharyngeal and hypoglossal nerves of the frog and observations of the alternatives produced thereby in the structure of their primitive fibers," Philos Trans R Soc Lond Biol. **140**, 423 (1850).
24. B. Beirowski,R. Adalbert, D. Wagner, D.S. Grumme, K. Addicks, R.R. Ribchester and M.P. Coleman, "The progressive nature of Wallerian degeneration in wild-type and slow Wallerian degeneration (WldS) nerves," BMC Neurosci. **6** (6), (2005).
25. A. Rosenfeld, M. Lorenz, R. Stoian and D. Ashkenasi, "Ultrashort-laser-pulse damage threshold of transparent materials and the role of incubation." Appl. Phys. A **69** [Suppl.], S373-S376 (1999).
26. Y. Lee, M.F. Becker and R.M. Walser, "Laser-induced damage on single-crystal metal surfaces." J. Opt. Soc. Am. B Vol.5 No.3, 648-659 (1988).

1. Introduction

Despite presenting significant technical challenges, nerve regeneration and degeneration studies hold great medical promise. It is estimated that currently nearly 5 million people suffer from degenerative diseases in the United States and the extensive medical treatment of these patients costs $100 billion per year to the healthcare system. Research towards understanding and curing these complex neurodegenerative diseases will have a huge economic and social impact [1].

Nerve regeneration involves complicated bio-molecular processes. As such, the interplay of these processes is best examined within a simple organism and using a precise non-invasive surgical cutting tool. The latter will determine the minimal size of the organism that can be studied. Since precision techniques for severing axons (axotomy) were not available until recently, previous works on nerve regeneration have often relied on using micro-needles for axotomy and have been conducted on large complicated organisms such as mice and zebrafish [2,3]. Alternatively, there is a great interest in studying nerve regeneration in the roundworm *Caenorhabditis elegans* (*C. elegans*) because of its simplicity as an invertebrate organism having only 302 neurons and also because of the availability of extensive genetic tools [4]. We have recently demonstrated that femtosecond (fs) laser pulses can be used as precise cutting tools for severing axons in *C. elegans* and that the operated axons can regenerate and recover their functionality after the operation [5]. This first demonstration of the existence of spontaneous nerve regeneration in a model organism has opened a new frontier for the nerve regeneration studies that can be performed using the highly precise and non-invasive cutting tool "fs-laser nanoaxotomy".

Such high precision laser surgery relies on highly localized ablation using ultra-short laser pulses [6-8]. High peak intensities and the nonlinear absorption of ultra-short laser pulses by the biological tissue allow for very low energy pulses to be used (down to a couple of nano-Joules using tight focusing). With limited collateral damage in surrounding tissue during axotomy, it is now possible to follow up regeneration processes and screen-test drugs and other biomolecules. Other groups have also shown that low energy fs-laser pulses are precise enough, for example, to dissect chromosomes with sub-micron resolution, transfect DNA inside cells or ablate subcellular structures such as mitochondria and cytoskeleton [9-14].

The neural regeneration process can be impaired by the amount of collateral damage caused by the laser ablation. Such damage can extend beyond the submicron focal volume of the laser beam as a result of expanding laser-induced plasmas and cavitation bubbles. In our previous work on nerve regeneration, the axonal recovery rate in motor neurons was

determined to be 54% and the functional recovery was observed in only 2 out of 17 worms. The question remained as to how much of this recovery is directly impaired by the laser axotomy that was performed. Were these statistics determined by the laser parameters (laser energy and number of pulses) or is nerve regeneration success inherent to the bio-physiology of the nematode? Studying the extent of laser-induced photo-damage and its effect on regeneration probability as a function of the laser parameters allow us to understand the role of the fs-laser nanoaxotomy on the regeneration process and therefore control its precision.

The extent of damage by fs-laser pulses at 1kHz repetition rate has previously been investigated on subcellular structures: actin filaments and nuclei using transmission electron microscopy (TEM) [12]. Depending on the type of cell on which surgery was performed, it was shown that the damage threshold for 1000 laser pulses focused with a 1.4 NA lens was between 1nJ and 1.7 nJ.. The size of the damage on actin filaments increased from 240 nm at 2.2 nJ to 600 nm at 4.4 nJ.

In this paper, we present a study on the probability of the axonal recovery of injured touch neuron processes as a measure for the precision of the fs-laser nanoaxotomy and the resultant extent of the damage. Here, we will use the term "axonal recovery" to indicate those injured axons that can regrow and reconnect to their distal end within 24 hours. Both of these processes greatly depend on the extent of damage incurred during the surgery. The goal of this paper is to find the optimal ablation conditions that will not impair the axonal recovery.

2. Experiments

2.1 Samples

The roundworm *C. elegans* is the first multicellular organism to have had its complete cell lineage established [15]. Its simple and invariant anatomy (981 cells comprising 302 neurons in the adult hermaphrodite) has appealed to scientists in genomics, cell biology, neuroscience, and aging. It is relatively easy to breed *C. elegans* due to its short life cycle and simple diet (*Escherichia coli* bacteria).

Two *C. elegans* transgenic strains presented in Fig. 1 were used in the present studies. The first strain, CZ5062 = *juIs76* (punc-25::GFP)II; *stEx37* (PAT-2::GFP); *lin-15*(*n765ts*)X, has 19 GABA-ergic motor neurons (D type) labeled with green fluorescent protein (GFP) as well as the myosin filaments of the underlying muscles (Fig. 1(a)) [16]. The VD and DD motor neurons are located in the ventral cord with circumferential processes extending to the dorsal cord. Axotomy is performed on these circumferential axons in areas where the muscles are also fully exposed, i.e. at around ¼ or ¾ of their length (see insert). All measurements of damage threshold and extent of damage were performed on that strain.

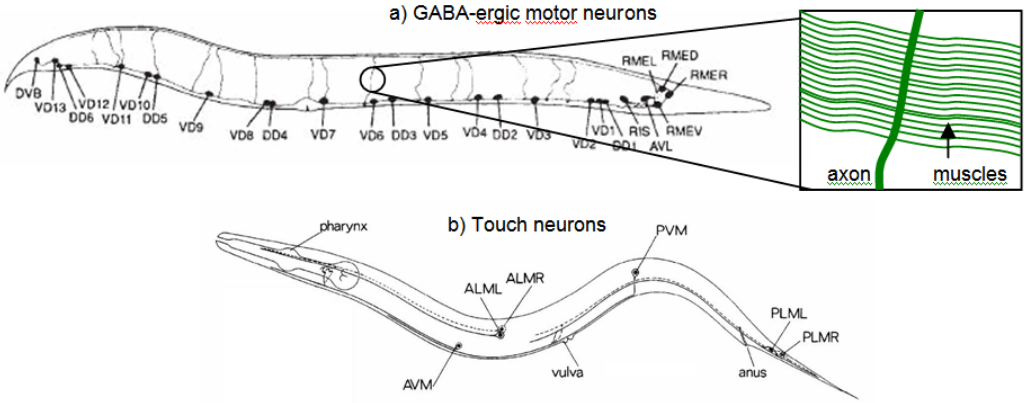

Fig. 1. a) Sketch of all GABA-ergic neurons in *C. elegans* (head to the right). The 13 VDs and the 6 DDs are the motor neurons. The insert shows myosin filaments underlying an axon [17]. b) Sketch of soft touch neurons in *C. elegans* (head to the left) [18]. ALM and PLM come in pairs; only one of each is accessible during surgery.

Axonal recovery studies were performed in a second transgenic strain, *zdIs5*(mec-4::GFP) that expresses the touch neurons ALM, PLM, AVM, and PVM with GFP (Fig. 1(b)) [19]. These neurons have long longitudinal processes running laterally beneath the cuticle alae. The worms crawl on their left or right side (never on the ventral side), always exposing either the left or right neurons of the ALM and PLM pairs. The mechanosensory processes have a mixed identity of axon and dendrite. For simplicity, they are referred to as axons in this paper.

All worms were anesthetized by phenoxy-propanol (5µl per ml of agar) and underwent surgery during the last larval stage (L4) of their life cycle. By the time they were observed for axonal recovery, namely after 24 hours, they had reached the young adult stage.

2.2 Experimental Setup

Figure 2 shows the experimental setup that incorporates nanosurgery capability using a fluorescence microscope. The surgery beam is delivered by a regenerative Ti-Sapphire amplifier (Spectra Physics, "Spitfire") seeded by a mode-locked tunable Ti-Sapphire (Spectra Physics, "Tsunami"). The pulses generated at 1 kHz repetition rate, have 220 fs pulse widths, 780 nm wavelength, and 1 mJ of maximum pulse energies. The energy is attenuated using two sets of a half wave plate (HWP) and a polarizing cube beam-splitter (CBS). To obtain pulses of a couple of nano-Joules, we also added a reflective filter with an optical density of 1.0. Pulse energies are measured by an energy meter (Ophir PL10) near the focal point of the surgery beam. The laser beam is then tightly focused on the target through an oil-immersion objective lens (Zeiss, 63x, NA=1.4). The surgery beam fills the back aperture of the objective lens. The spot size is estimated to be about 620 nm based on the theoretical $1/e^2$ diameter of focused Gaussian beams ($0.925\ \lambda/NA$) [20] and the measured "*M*-squared" parameter (M^2 =1.2±0.1). The pulse duration at the sample at is estimated to be 430 fs. This estimate is performed using a two-photon absorption collinear autocorrelator with a photodiode (G1117, Hamamatsu) and an objective lens group delay dispersion value of 3520 fs^2 [21].

The fluorescence imaging system consists of a mercury lamp (Nikon XCite 120), an FITC filter set and a cold mirror which transmits the laser beam but reflects both the excitation light and the fluorescence emission. Images are recorded by a CCD camera (Photometrics, CoolSnap ES) with an exposure time of 200 ms.

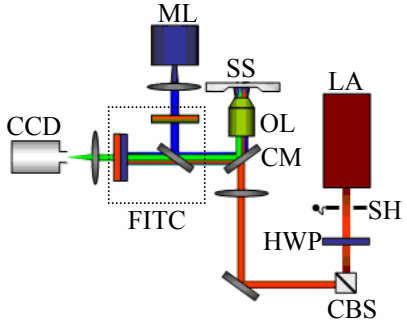

CBS – Cube beam-splitter (polarizing)
CM – Cold mirror
HWP – Half wave plate
ML – Mercury lamp
SH – Shutter
CCD – Digital camera
FITC – Fluorescein Isothiocyanate filter set
LA – Laser (femtosecond)
OL – Objective lens
SS – Sample stage

Fig. 2. Setup where nanosurgery is incorporated in a fluorescence microscope.

3. Results and discussion

3.1 Axonal recovery (regrowth and reconnection)

In our recent paper, we have established that nerve regeneration occurs with functional recovery in motor neurons of *C. elegans* [5]. We also observed that injured axons of touch neurons can regrow and reconnect to their distal end [22]. Figure 3 shows an example for the

axonal recovery (regrowth of proximal end and its reconnection to distal end) of a PLM left (PLML) touch neuron. Right after the surgery, the proximal and distal ends of the worm were about 2 μm apart as observed by the disappearance of the GFP signal in Fig. 3(b). After 12 hours, the proximal end regrew and reconnected with the distal end (Fig. 3(c)).

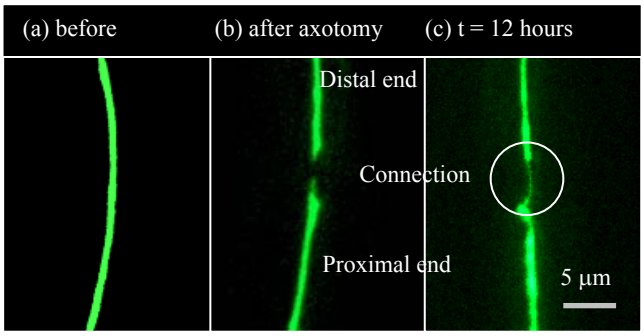

Fig. 3. Fluorescence images of an axon of a GFP-labeled PLML neuron (a) before axotomy, (b) right after the axotomy at mid-body (100 pulses of 1.9 J/cm^2), and (c) 12 hours after the axotomy showing regrowth of the severed axon and reconnection to its distal end.

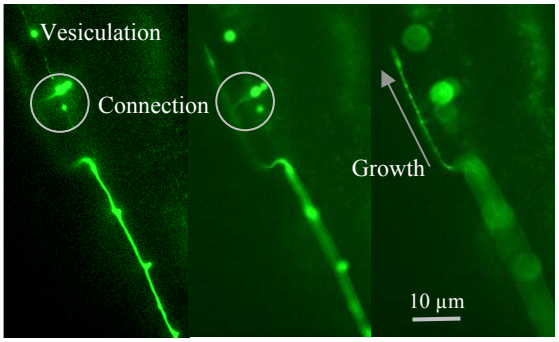

Fig. 4. Images of regrown ALML axon 72 hours after axotomy on a youg adult worm (300 pulses of 1.9 J/cm^2) at three different focal depths. The first two images show the connection to the degenerated distal end and the third image shows how the process continues to regrow most probably in search of a healthier connection. (The distal and proximal ends are respectively on the upper and lower parts of the pictures).

It is important to note that we can identify the unsuccessful reconnections in some cases by observation of the morphology of the recovering axons. For example, Fig. 4 presents an axon which has reconnected to an unhealthy distal end. In this case, the axon cannot reestablish appropriate information trafficking with its target. The three images in Fig. 4 show the same axon 72 hours after axotomy at different focal depths in order to follow the morphology of the grown axon. In the first image, the distal end is clearly vesiculated, which is indicative of Wallerian degeneration [23,24]. The connection is visible inside the circle on the first and second images. The third image clearly shows that the axon did actually continue to grow after connection to the degenerated distal end in search of a healthy one. In this experiment the axon regrowth was slow and the reconnection only happened after the Wallerian processes have started. The slow regrowth of the process was due to the age of the worms, already young adults at the time of the surgery.

Moreover, if the distal end has not connected before Wallerian degeneration has started, it will irremediably degenerate as shown in Fig. 4. In summary, investigation of the recovery (regrowth and successful reconnection) of laser axotomized axons can provide valuable insight on how the resultant extent of photo-damage affects the regeneration process in *C. elegans*.

3.2 Photobleaching versus ablation.

When a GFP labeled axon is irradiated with fs-laser pulses of a certain energy level, we observe a loss in its fluorescence, which does not always correspond to removal of material (ablation). At energy levels below the damage threshold, the axon may lose its GFP signal due to photobleaching without causing ablation. Figure 5 perfectly illustrates the photobleaching effect. Right after laser exposure using 25 pulses of 1.3 J/cm^2, the axon loses its GFP signal, which could be interpreted as permanent damage. After two minutes, however, its luminescence is restored by GFP diffusion within the cytoplasm of the intact axon. The underlying muscle fibers (less than 1 μm beneath the axon) do not seem to have been photobleached. The reason is that the focal depth of the setup is large enough to image myosin fibers that have not been exposed to the laser.

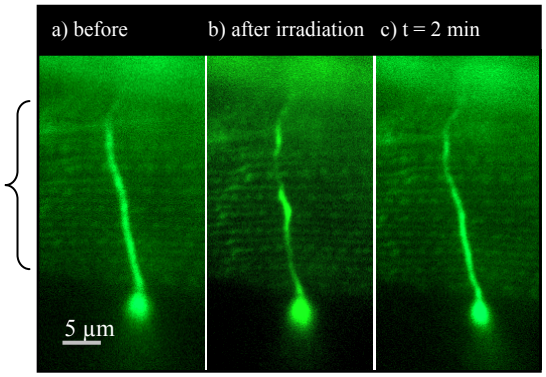

Fig. 5. Fluorescence images of photobleaching at 1.3 J/cm^2, 25 pulses on CZ5062 , (a) before laser exposure, (b) right after exposure, and (c) 2 minutes after exposure. The irradiated spot loses its signal due to photobleaching but remains intact. The axon recovers its luminescence within 2 minutes by the GFP diffusion within the cytoplasm.

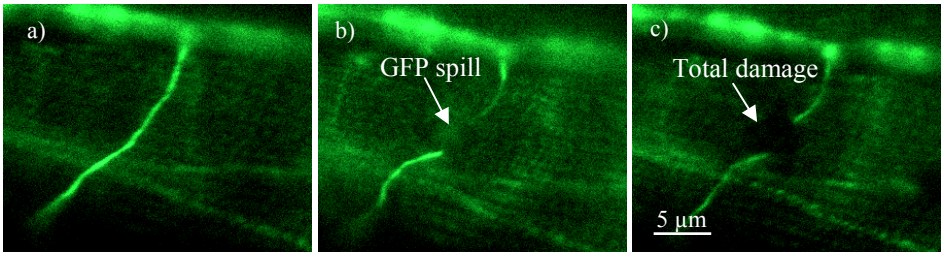

Fig. 6. Fluorescence images of the extent of damage induced by fs-laser ablation using 800 pulses at 1.7 J/cm^2. (a) before ablation, (b) right after ablation with GFP spilling in the created cavity, and (c) 3 minutes after ablation. The dark region in muscle fibers shows the extent of damage to surrounding tissue. The diameter of this area is approximately equal to the distance between the ends of the cut axon.

Figure 6 shows that at higher pulse energies beyond the damage threshold, the loss of GFP signal is permanent and the luminescence is not recovered. At these energy levels both photobleaching and ablation may occur. Right after axotomy, the cellular plasma containing the GFP spills in the cavity (Fig. 6(b)). Within seconds, both the proximal and distal ends of the axon seal themselves and luminescence is restored in the remaining intact axon. The photobleached region, if any, would be restored after sealing. There is also possible retraction in the proximal and distal ends of the axons beyond the cut until sealing is complete. We have used the distance in between the sealed axons as a measure of the extent of total damage, namely removal of material due to laser ablation and retraction if any. The dark region in muscle fibers shows the extent of damage to surrounding tissue (Fig. 6(c)). We did not observe any luminescence recovery in these fibers. Unlike the cytoplasmic GFP of the neurons, circulating freely in the cell, the GFP in the muscle fibers are embedded in the

myosin. Therefore, a fluorescence recovery would take much longer due to slower diffusion rate.

3.3 Damage threshold.

We measured the damage threshold, namely the minimum energy required to observe permanent damage for each pulse train applied to the sample. Starting at a pulse energy of 0.8 nJ, the energy was increased until an optically detectable permanent cut (around 1 μm in size) could be observed. The target location on the axon was changed each time in order to avoid accumulative effects. Each set of data represents an average value of ablation thresholds measured in 10 different axons of several worms.

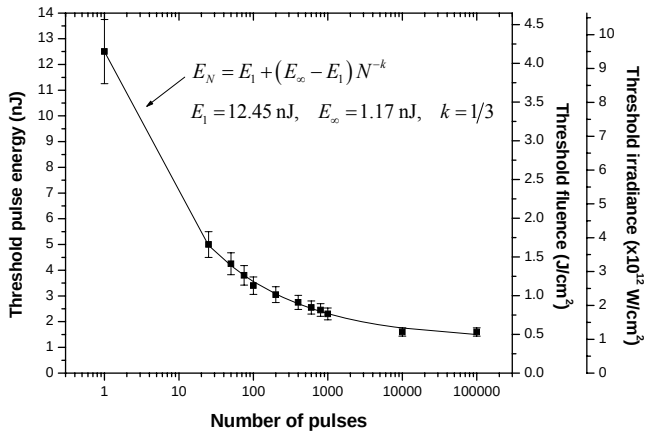

Fig. 7. Ablation thresholds measured as a function of number of pulses. Solid line shows the logarithmic fit following Eq. (2). The corresponding fluences (energy per area) and irradiances are included in the right side axis assuming a theoretical spot size of 620 nm and a pulse duration of 430 fs. The error bars indicate the variance of the threshold measurements on 10 axons for different pulse trains.

Figure 6 presents the measured damage threshold data. The damage threshold decreases monotonically as the number of pulses increases, until it reaches a plateau. This decrease can be the result of an incubation effect. To understand the factors leading to such an incubation effect, the role of various damage mechanisms involved in fs-laser ablation of tissue is needed to be discussed.

Table 1. Damage mechanisms in fs-laser nanosurgery at kHz repetition rate [8]. The irradiance thresholds and the free electron densities were estimated by Vogel et al. for 100 fs, 800 nm laser pulses focused with 1.3 NA lens [8].

Damage mechanism	Photochemical Damage	Thermoelastic Stress Confinement	Plasma-Mediated Ablation
Irradiance threshold	0.26×10^{12} W/cm^2	5.1×10^{12} W/cm^2	6.54×10^{12} W/cm^2
Electron density per pulse	2.1×10^{13} cm^{-3} low density plasma regime	0.24×10^{21} cm^{-3} low density plasma regime	1.0×10^{21} cm^{-3} dense plasma regime
Description	Free electrons participate in chemical reactions to form destructive reactive oxygen species and lead to breaking of chemical bonds.	Since thermalization of the plasma occurs faster than the acoustic relaxation time, confinement of thermal stresses leads to formation of nano-scale transient bubbles.	The damage is created by the extremely hot plasma and the accompanying shock wave and cavitation bubble.

Above a certain laser irradiance (0.26 x 10^{12} W/cm^2), the absorption of fs-laser pulses produces free electrons through multiphoton ionization, electron tunneling, cascade ionization and electron diffusion [8]. Depending on the density of these free electrons, several different damage mechanisms can lead to the dissection effect of tissue at the kHz laser repetition rate [8]. A summary of these damage mechanisms is provided in Table 1.

Plasma-mediated ablation occurs above an irradiance threshold of 6.54 x 10^{12} W/cm^2, when a very high free electron density is formed. In that case, the damage is created by the extremely hot plasma and the accompanying shock wave and cavitation bubble. The single-pulse nanosurgery, having a threshold irradiance of 9.63 x 10^{12} W/cm^2, may therefore be the result of a plasma-mediated ablation. At lower irradiances, yielding a lower free electron density (low density plasma regime), the damage occurs due to thermo-elastic stress induced nanometer scale transient bubbles [8]. However, a nanometer scale damage would not be sufficient to sever axons which are about 300 nm in diameter. In this case, it will also be impossible to detect any damage using fluorescence imaging. Multiple laser pulses can eventually lead to a larger damage size due to the accumulative defects, generated after relaxation of the transient bubbles. That may be the case for our threshold measurements using multiple pulses.

In the low density plasma regimes, the free electrons may also participate in chemical reactions to form destructive reactive oxygen species and free radicals that in turn help in the breaking of chemical bonds. Accumulation of this effect may eventually contribute to the disintegration of the axon and lower the ablation threshold.

We call these accumulative effects "incubation". Several groups studied the incubation effect on ultrashort laser pulse damage on dielectrics and metals [25,26]. They described the dependence of fluence threshold on the incubation effect according to [26]:

$$F_N = F_1 + \left(F_\infty - F_1\right) N^{-k}, \tag{1}$$

where N is the number of pulses, F_1 and F_∞ are the fluence threshold for a single shot and for an infinite number of pulses, respectively. The parameter k describes the strength of the incubation effect, related to the thermal stress fatigue in the case of metals [26] or to charge transfers due to impurities and vacancies in dielectrics [25]. Replacing fluence with pulse energy we obtain

$$E_N = E_1 + \left(E_\infty - E_1\right) N^{-k}. \tag{2}$$

The fitting of our threshold data to this equation yields a dependency of the fluence threshold to the inverse of the cubic root of the number of pulses (k = 1/3). Here, in the case of tissue ablation, k is most probably related to the accumulation of chemical dissociation effects as well as to the defects (impurities and vacancies) created by the nanometer scale transient bubbles.

When multiple pulses of energies high above the damage threshold are used both of these damage mechanisms may eventually result in large and long lived (hundreds of milliseconds) cavitation bubbles due to accumulative effects. Such an accumulative cavitation phenomenon was observed in our experiments for energies above 5.5 nJ (4.24 x 10^{12} W/cm^2) when using 400 pulses or more.

3.4 Extent of damage

Figure 8 summarizes the extent of photo-damage measured as the distance between the proximal and distal ends of the severed axons after they are sealed. As discussed in section 3.2 this measurement indicates mainly the size of the damaged area although there may be some retraction of the axons until they are sealed. The measurements of photo-damage resulted in similar sizes of damage (within the error bars) for a given laser fluence.

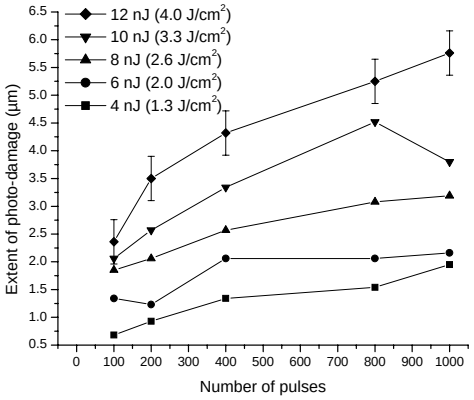

Fig. 8. Extent of photo-damage induced by fs-laser ablation of axons in *C. elegans* as a function of pulse energy and total number of pulses.

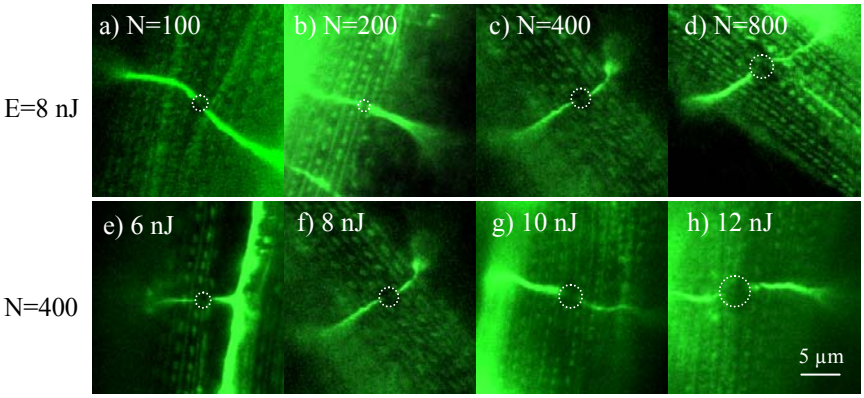

Fig. 9. Fluorescence images of the extent of damage, (a-d) at 8 nJ for 100, 200, 400 and 800 pulses, (e-h) for 400 pulses at 6, 8, 10 and 12 nJ.

For each energy level, there is a minimum number of pulses that will initiate ablation. For example, at 1 nJ per pulse, there is no ablation even for 100,000 pulses (100 seconds of laser exposure) while at 2.2 nJ per pulse, ablation is observed by using as few as a 1,000 pulses. Once ablation is initiated the amount of photo-damage does not increase substantially with increasing numbers of pulses (Fig. 9(a-d)). On the other hand, for each number of pulses, the damage increases rapidly with pulse energy (Fig. 9(e-h)).

A statistical evaluation of the error for the damage size was completed based on the ablation of 10 different axons of several worms. When using more than 100 pulses, the size of the extent of damage varied slightly (0.3-0.4 µm) from experiment to experiment. For clarity, error bars were added to the graph for one energy level only.

3.5 Axonal recovery statistics.

In order to determine the effects of the extent of damage on regrowth and reconnection of axons to their distal end, we studied how the injured axons of touch neurons are recovered for different pulse energies and number of pulses. For regeneration to be complete, the axonal recovery of injured axons must eventually lead to a functional recovery of the neuron. Functional recovery of touch neurons can be tested by observing the sensitivity of recovered worm to soft touch. In the present study, we did not test the functional recovery of touch neurons because the surgery was performed on one side of the worm only. However as we discussed in section 3.1, the investigation of the axonal recovery provides valuable insight on how the laser parameters and the resultant extent of damage affect the regeneration process in *C. elegans*. The results are summarized in Fig. 10. The actual values are presented in Table 2.

Whether the axotomy was performed with 400 pulses of 2.5 nJ or with 100 pulses of 10 nJ, dramatic changes were observed in axonal recovery even though the total deposited energy remains 1 μJ .

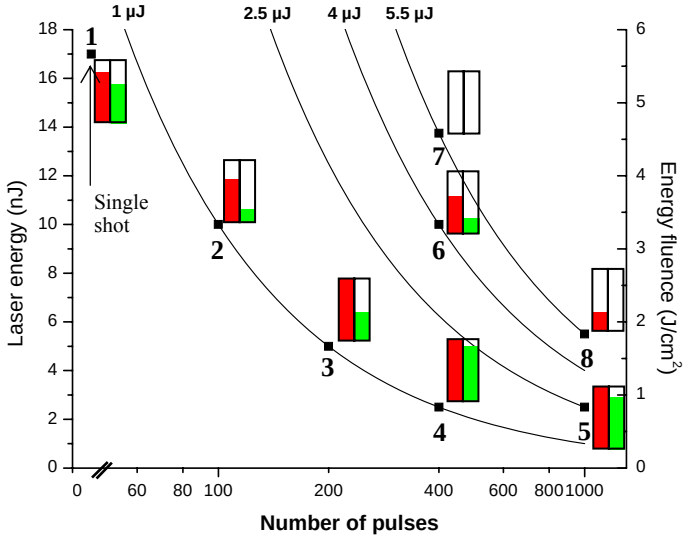

Fig. 10. Axonal recovery probabilities of touch neurons. Red bars on the left are survival rates after anesthesia and surgery. Green bars on the right are axonal recovery rates.

Table 2. Statistics of axonal recovery of touch neurons and survival rate of worms after laser axotomy performed using different pulse energies and total number of pulses. Relative rates refer to the number of worms fulfilling the requirement of the previous column.

Exp. #	Total energy μJ	Pulse energy nJ	Number of pulses	Burst of the cuticle	Survival rate		Axonal recovery	
					relative	total	relative	total
1	0.017	17	1	0%	80%		80%	65%
2	1	10	100	0%	70%		28%	20%
3	1	5	200	0%	100%		47%	
4	1	2.5	400	0%	100%		90%	
5	2.5	2.5	1000	0%	100%		85%	
6	4	10	400	10%	66%	60%	42%	25%
7	5.5	13.75	400	100%	0%		0%	
8	5.5	5.5	1000	40%	50%	30%	0%	

Severed axons showed regrowth in all cases and a complete recovery (regrowth and reconnection) in some cases. We found that the axonal recovery rate depends greatly on the amount of pulse energy used and the way it was delivered. To establish statistical results for the axonal recovery studies, we considered a population of 10 individual worms (i.e. 20 neurons) at L4 stage for each set of laser axotomy conditions. Using the ANOVA test (ANalysis Of VAriance) we determined that the observed dependence of both survival and axonal recovery rates on the laser parameters (pulse energy and number of pulses) is statistically significant ($P < 0.001$, 160 axons).

The analysis of these statistics combined with the results of the extent of damage reveals the following conclusions:

1. Experiment 1. With a single pulse of 17 nJ, the size of the apparent photo-damage is very small. Yet the probability of axonal recovery is only about 65%. This means that the cavitation bubble created by that single pulse induces a large enough structural damage to surrounding tissue, inhibiting to some extent proper regeneration processes.

2. Experiments 2, 3 and 4. For the same amount of total energy, the probability of axonal recovery can significantly be improved (from 20% to 90%) using larger number of pulses with lower pulse energies. This result is consistent with the trend of the extent of damage decreasing from about 2 μm to about 1 μm. Of course, using lower total energy guarantees better odds of axonal recovery success, in general.
3. Experiments 2 and 6 or 4 and 5. If the laser pulse energy is held constant, the probability of axonal recovery gets slightly reduced as the total energy is increased, i.e. as the number of pulses is increased.
4. Experiments 4, 6 and 7. Holding the number of pulses constant, the probability of axonal recovery dramatically improves when the laser energy is reduced. Reducing the energy per pulse by a factor of 3 increases the probability of recovery from 0% to 90%. Once again the same trend is observed in terms of extent of damage (Fig. 8): increasing the energy per pulse by a factor of 3 (from 4 nJ to 12 nJ) increases the extent of damage by 3-4 times (from about 1.3 μm up to 4.4 μm).

In single shot experiments, where higher energy is needed to reach the damage threshold, the induced cavitation bubble will cause larger structural damage to surrounding tissue, increasing the odds of bursting the cuticle. As shown in Fig. 7, due to variations in light scattering from worm to worm (variations in the cuticle, alae, and the amount of accumulated bacteria), small number of pulses (below 100) cause higher variability both in the ablation threshold and in the extent of damage. In contrast, the nano-axotomy process is highly repeatable when using large number of pulses (above 100) with low energies, for example, 200 pulses of 5 nJ. In addition to high repeatability, low energy pulse trains (experiments 3, 4, and 5) provide the experimentalist the ability to control the axonal recovery rates. Depending on the kind of screen-test performed, whether the drug or molecule is inhibitory or inductive, the experimentalist can adjust the statistical rate of axonal recovery from 50% to 90%.

4. Conclusion

We investigated the effect of laser parameters on the extent of damage induced by fs-laser nanosurgery on axons of *C. elegans* and the resulting axonal recovery rates. We first determined the energy levels necessary for a permanent damage in axons. We showed that the damage threshold decreases with the increasing number of pulses applied to the sample as a result of an incubation type effect. The measured values of irradiance thresholds correlated well with those calculated by Vogel et al. [18] providing an insight on the possible ablation mechanisms involved during fs-laser nanoaxotomy.

We then studied the dependence of the extent of the damaged region on laser parameters. The amount of energy per pulse is found to have a larger effect on the size of the damaged area than the number of pulses applied.

Finally, we examined the effect of laser parameters on axonal recovery (regrowth and reconnection to the distal end) rates. Interestingly, the lowest total energy deposition during surgery does not guarantee the highest rate of recovery. Nonetheless, for high success rates, it is preferable to use laser energies near the damage threshold and pulse trains above 100 pulses. Using low energy pulse trains will allow us in the future to control surgery conditions for which most worms will survive and yet only a portion of the severed axons will regenerate. In screen-testing of drugs or biomolecules, a comfortable statistical variability will ensure a more accurate interpretation of the results.

Acknowledgements

The work was supported by the NSF through Grant BES-0548673. We thank Dr. Yishi Jin for providing the CZ5062 and *juIs76* strains and Dr. Massimo Hilliard for providing the *zdIs5* strain and for his valuable input to this work. We also thank Alexis Crawley and Niraj Badhiwala for their constant care of the worms and the preparation of the samples.